Inorganic Chemistry
Article

Inorg. Chem. **2010**, *49*, 11449–11462 **11449**
DOI: 10.1021/ic1013945

Hydrothermal Synthesis and Characterization of 2D M(II)-Quinate (M = Co,Zn) Metal−Organic Lattice Assemblies: Solid-State Solution Structure Correlation in M(II)-Hydroxycarboxylate Systems

M. Menelaou,[†] A. Konstantopai,[†] N. Lalioti,[‡] C. P. Raptopoulou,[§] V. Psycharis,[§] A. Terzis,[§] C. Mateescu,[∥] K. Tsarhopoulos,[⊥] P. Rigas,[#] and A. Salifoglou*[,†]

[†]*Department of Chemical Engineering, Aristotle University of Thessaloniki, Thessaloniki 54124, Greece,* [‡]*Department of Chemistry, University of Patras, Patras 26500, Greece,* [§]*Institute of Materials Science, NCSR "Demokritos", 15310 Aghia Paraskevi, Attiki, Greece,* [∥]*Banat University of Agricultural Sciences and Veterinary Medicine, Timisoara 300645, Romania,* [⊥]*Rigas Laboratories S.A., Thessaloniki 54626, Greece, and* [#]*Biotoxins and Analytical Chemistry Laboratory, Department of Fisheries and Aquaculture Technology, Technological Educational Institute of Thessaloniki, N. Moudania, Greece*

Received July 13, 2010

Co(II) and Zn(II) ions exhibit variable reactivity toward O-containing ligands in aqueous media, affording isolable materials with distinct solid-state lattice properties. D-(−)-quinic acid is a cellular α-hydroxycarboxylate metal ion binder, which reacts with Co(II) and Zn(II) under pH-specific hydrothermal conditions, leading to the isolation of two new species $[Co_2(C_7H_{11}O_6)_4]_n \cdot nH_2O$ (**1**) and $[Zn_3(C_7H_{11}O_6)_6]_n \cdot nH_2O$ (**2**). Compound **1** was characterized by elemental analysis, spectroscopic techniques (FT-IR, UV−visible, EPR), magnetic studies, and X-ray crystallography. Compound **2** was characterized by elemental analysis, spectroscopic techniques (FT-IR, ESI-MS), and X-ray crystallography. The 2D molecular lattices in **1** and **2** reveal the presence of octahedral M(II) units bound exclusively to quinate in a distinct fashion, thereby projecting a unique chemical reactivity in each investigated system. The magnetic susceptibility and solid-state/frozen solution EPR data on **1** support the presence of a high-spin octahedral Co(II) in an oxygen environment, having a ground state with an effective spin of $S = 1/2$. Concurrent aqueous speciation studies on the binary Zn(II)−quinate system unravel the nature and properties of species arising from Zn(II)−quinate interactions as a function of pH and molar ratio. The physicochemical profiles of **1** and **2**, in the solid state and in solution, earmark the importance of (a) select synthetic hydrothermal reactivity conditions, affording new well-defined lattice dimensionality and nuclearity M(II)−quinate materials, (b) structural speciation approaches delineating solid state−aqueous solution correlations in the binary M(II)−quinate systems, and (c) pH-specific chemical reactivity in binary M(II)−quinate systems reflecting structurally unique associations of simple aqueous complexes into distinctly assembled 2D crystalline lattices.

Introduction

The Co(II) and Zn(II) metal ions have been widely involved in the design of metal−organic coordination polymers,[1] which have recently attracted considerable interest, mostly due to their supramolecular composition and versatile framework topologies as well as their potential applications as functional materials in molecular magnetism, catalysis, gas sorption, fluorescent sensing, and optoelectronic devices.[2]

Cobalt and zinc have been known as essential trace elements in human physiology.[3] Cobalt has been found in enzymatic systems such as the B_{12} coenzyme, vitamin B_{12},[4] and cobalt-containing metallohydrolases.[5,6] It has also been (a) reported to exert carcinogenic activity,[7,8] (b) shown to cause DNA strand breaks in animal cell cultures,[9] (c) linked to anemias,[10]

*Author to whom correspondence should be addressed. Tel.: +30-2310-996-179. Fax: +30-2310-996-196. E-mail: salif@auth.gr.

(1) Bowden, T. A.; Milton, H. L.; Slawin, A. M. Z.; Lightfoot, P. *Dalton Trans.* **2003**, 936–939.
(2) Zhang, G.; Yang, G.; Ma, J. S. *Cryst. Growth Des.* **2006**, *6*, 375–381.
(3) Leung, F. Y. *Clin. Biochem.* **1995**, *28*, 561–566.
(4) Santander, P. J.; Kajiwara, Y.; Williams, H. J.; Scott, A. I. *Bioorg. Med. Chem.* **2006**, *14*, 724–731.
(5) (a) Roderick, S. L.; Matthews, B. W. *Biochemistry* **1993**, *32*, 3907–3912. (b) Ben-Bassat, A.; Bauer, K.; Chang, S.-Y.; Myambo, K.; Boosman, A.; Chang, S. *J. Bacteriol.* **1987**, *169*, 751–757.
(6) Lippard, S. J.; Berg, J. M. *Principles of Bioinorganic Chemistry*; U. Science Books: M. Valley, CA, 1994.
(7) Lison, D.; De Boeck, M.; Verougstraete, V.; Kirsch-Volders, M. *Occup. Environ. Med.* **2001**, *58*, 619–625.
(8) Léonard, A.; Lauwerys, R. *Mutat. Res.* **1990**, *239*, 17–27.
(9) DeBoeck, M.; Kirsch-Volders, M.; Lison, D. *Mutat. Res.* **2003**, *533*, 135–152.
(10) Shreeve, W. W. *Exp. Hematol.* **2007**, *35*, 173–179.

Published on Web 11/17/2010

and (d) shown to exert toxic effects associated with elevated formation of red corpuscles and heart disease.[11,12] Zinc is one of the most important trace metal ions in all living organisms, influencing nutrition,[13] gene expression, and cell division.[14] As a metal, it enters a wide range of applications, including batteries,[15] alloys,[16] dye-casting,[17] dental materials,[18] etc. Consequently, both Co(II) and Zn(II) can interact with various molecular mass binders, entering binary and ternary interactions and affording unique complexes with distinct structural and spectroscopic properties. In this context, appropriately structured ligands bearing O-, N-, and S-containing anchors are excellent candidates to interact with Co(II) and Zn(II). α-Hydroxycarboxylic acids are such low molecular mass ligands poised to promote binding to Co(II) and Zn(II), forming soluble complexes. A representative α-hydroxycarboxylic acid binder is D-(−)-quinic acid, a precursor of shikimic acid,[19] which is involved in the biosynthesis of aromatic amino acids. It is a polyfunctional organic ligand containing two important structural features: (a) a carboxylate moiety known to promote metal ion binding and (b) alcoholic moieties, one of which is in an α position to the carboxylate group and three adjacently located alcoholic groups, akin to polyol functionalities.

Given the paucity of well-characterized binary M(II)−quinate (M = Co, Zn) materials of distinct structural and spectroscopic properties in the solid state and in solution, an in-depth investigation of the aqueous chemistry of Co(II) and Zn(II) with α-hydroxycarboxylic D-(−)-quinic acid could shed light on the respective binary interactions and physicochemical profile of (a) the emerging soluble species and (b) ultimately the isolated materials as a function of pH, molecular stoichiometry, and reaction conditions. To this end, we report herein (a) aqueous solution speciation studies on the binary Zn(II)−quinate system and the pH-specific synthesis, isolation, and structural characterization of the first trinuclear core-containing Zn(II)−(D-(−)-quinate) coordination polymer; (b) the synthesis, isolation, and structural characterization of the first dinuclear core-containing Co(II)−quinate polymer along with transformation studies associating all reported mononuclear Co(II)−quinate species with the aforementioned compound, and finally (c) the distinct physicochemical attributes of 2D M(II)−quinate crystal lattices along with solid-state-solution structure correlations.

Experimental Section

Materials and Methods. All manipulations were carried out under aerobic conditions. $Co(CH_3COO)_2 \cdot 4H_2O$ was purchased from RP Carlo Erba, D-(−)-quinic acid from Fluka, and $Zn(CH_3COO)_2 \cdot 2H_2O$ from Merck. Nanopure-quality water was used for all reactions run.

Physical Measurements. FT-infrared measurements were taken on a 1760X FT-Infra Red spectrometer from Perkin-Elmer, using KBr pellets. UV/visible measurements were carried out on a Hitachi U2001 spectrophotometer in the range 190−1000 nm. A ThermoFinnigan Flash EA 1112 CHNS elemental analyzer was used for simultaneous C, H (%) determination.

ESI-MS infusion experiments were carried out by using a ThermoFisher Scientific (Bremen, Germany) model LTQ Orbitrap Discovery MS. All aqueous solutions (A = Zn(II) and B = quinic acid, 10^{-2} M each, mixed in molar ratios A/B of 1:1 and 1:2) were introduced into the ESI source of the MS at a flow rate of 3 μL/min by using an integrated syringe pump. The infusion experiments were run using a standard ESI source operating in a positive ionization mode. Source operating conditions were as follows: 3.7 kV spray voltage, 275 °C heated capillary temperature, and 8 psi sheath gas pressure. Full scan MS analysis was performed in profile mode, using the Orbitrap mass analyzer at a mass resolving power of 30 000 (fwhm, at m/z 400), followed by data-dependent MS/MS on the top five most intense ions from the full scan. Data-dependent MS/MS analysis was performed in parallel with the MS analysis, in centroid mode, using the LTQ mass analyzer. All accurate mass measurements of the [M + H] ions were carried out by scanning from 150 to 500 m/z. Automatic gain control (AGC) of the linear ion trap was switched on. The AGC target value was 30 000 accumulated ions for the linear ion trap and 500 000 accumulated ions for the Orbitrap. The Orbitrap was calibrated before the infusion experiments by using a mixture of caffeine, MRFA peptide, and Ultramark 1600. Data were acquired in an external calibration mode. The Mass Frontier (HighChem, Slovakia) software was used to confirm a suggested compound identity and structure based on observed fragmentation patterns.

The EPR spectra of complex **1** in the solid state and in frozen aqueous solutions were recorded on a Bruker ER 200D-SRC X-band spectrometer, equipped with an Oxford ESR 9 cryostat at 9.61 GHz, 10 dB (2 mW), and 4 K. Magnetic susceptibility data were collected on powdered samples of **1** with a Quantum Design SQUID susceptometer in the 3.0−290.0 K temperature range, under various applied magnetic fields. Magnetization measurements were carried out at three different temperatures in the field range 0−7 T.

pH-Potentiometric Measurements. The protonation constants of quinic acid were determined by pH-potentiometric titrations of 30 mL samples in the pH range 2.8−13.0 under a purified Ar atmosphere. The concentration of quinic acid was in the range of 1.7−7.0 mmol dm^{-3}. The stability constants of the complexes between Zn(II) and quinic acid were determined by pH-potentiometric titrations of 30 mL samples in the pH range 3.3 to 7.9−8.2, at which point $Zn(OH)_2$ began to precipitate. The samples were, in all cases, completely deoxygenated by bubbling purified Ar for 10 min before the measurements. Ar was also passed over the solutions during the titrations. The final pH depends on the zinc/ligand molar ratio. Precipitation was observed at a pH of ∼7.9−8.2, in line with the previously reported behavior of the aqueous system of Zn(II) with orotic,[20] 2-hydroxynicotinic, and 3-hydroxypicolinic acids;[21] N-acetyl-His−Pro−His−His−NH_2;[22] and some aminodiphosphonic acids.[23]

(11) Helis, H. M.; DeMeester, P.; Hodgson, D. J. *J. Am. Chem. Soc.* **1976**, *99*, 3309–3312.
(12) Waldbott, G. L. *Health Effects of Environmental Pollutants*; Mosby, C. V. Co.: St. Louis, MO, 1973.
(13) Lee, Y. M.; Lim, C. *J. Mol. Biol.* **2008**, *379*, 545–553.
(14) Amin, A. S.; Issa, Y. M. *J. Pharm. Biomed. Anal.* **2003**, *31*, 492–497.
(15) Vatistas, N.; Bartolozzi, M.; Arras, S. *J. Power Sources* **2001**, *101*, 182–187.
(16) Nilsson, A.; Gabrielson, P.; Stahl, J. E. *J. Mater. Process. Technol.* **2002**, *125*, 806–813.
(17) Nakagawa, J.; Matsuoka, M. *Environ. Tox. Pharm.* **2008**, *26*, 109–112.
(18) Kalicanin, B. M.; Nikolić, R. S. *J. Trace Elem. Med. Biol.* **2008**, *22*, 93–99.
(19) (a) Haslam, E. *Shikimic Acid: Metabolism and Metabolites*; Wiley & Sons: New York, 1993. (b) Pittard, A. J. *Escherichia coli and Salmonella: Cellular and Molecular Biology*; Neidhardt, F. C., Ed.; ASM Press: Washington, DC, 1996.
(20) Hacht, B.; Tayaa, H.; Benayad, A.; Mimouni, M. *J. Sol. Chem.* **2002**, *31*, 757–769.
(21) DiMarco, V. B.; Tapparo, A.; Dolmella, A.; Bombi, G. G. *Inorg. Chim. Acta* **2004**, *357*, 135–142.
(22) Kurzak, B.; Kozlowski, H.; Decock, P. *J. Inorg. Biochem.* **1991**, *41*, 71–78.
(23) Kurzak, B.; Kamecka, A.; Kurzak, K.; Jezierska, J.; Kafarski, P. *Polyhedron* **2000**, *19*, 2083–2093.

All solutions were prepared using Fluka reagent-grade quinic acid, $Zn(NO_3)_2 \cdot 6H_2O$, and ultrapure deionized water. The purity of quinic acid and the exact concentration of quinate were determined by the Gran method.[24] The Zn(II) solution was calibrated with standard ethylene diamine tetraacetic acid (EDTA).[25]

The ionic strength was adjusted to 0.15 M with NaCl, and the temperature was maintained at 25.0 ± 0.1 °C during the measurements. The titrations were carried out with a carbonate-free NaOH solution of a known concentration (ca. 0.15 M). The NaOH solution was standardized using potassium hydrogen iodate ($KH(IO_3)_2$). The ligand concentration was 4 mM, and the employed metal/ligand ratios were 1:1, 1:2, 1:3, and 1:4. The pH was monitored with a computer-controlled Crison titration system elaborated for titrations at such low concentrations[26] and a Mettler Toledo-Inlab 412 combined glass-electrode, calibrated for hydrogen ion concentration according to Irving et al.,[27] by using the GLEE program.[28] The ionic product of water was found to be $pK_w = 13.76$.[29]

The stepwise protonation constants of quinic acid are given as $\log K_n$ (n = 1,2), consistent with the equilibrium $H_{n-1}L + H \rightleftarrows H_nL$, where $K_n = [H_nL]/[H_{n-1}L][H]$. The initial computations were obtained in the form of overall protonation constants $\beta_n = [H_nL]/[L][H]^n$, taking into account that $\beta_n = \Pi_{n=1}^{n=2} K_n$. The concentration stability constants $\beta_{pqr} = [M_pL_qH_r]/[M]^p[L]^q[H]^r$ for quinic acid were calculated with Superquad,[30] and for Zn(II)−quinate complexes, emerging in the investigated system, with the PSEQUAD computer program.[31] Species distribution diagrams were computed from the overall formation constants with HySS.[32]

The formation of hydroxo complexes of Zn(II), and $[ZnH_{-1}]^+$,[21] was taken into consideration in the employed calculations. The stability constant used for the monohydroxo species of Zn(II) was taken from the data of Reichle et al.[33] and corrected for an ionic strength of 0.15 M, using the Davies equation: $[ZnH_{-1}]^+$ ($\log \beta_{1-1} = -8.08$).[34]

Synthesis of $[Co_2(C_7H_{11}O_6)_4]_n \cdot nH_2O$ (1). $Co(CH_3COO)_2 \cdot 4H_2O$ (0.80 g, 3.2 mmol) and D-(−)-quinic acid (1.2 g, 6.5 mmol) were placed in a 25 mL round-bottom flask and dissolved in 4 mL of water. The pH of the arising solution was ∼5. The reaction mixture was then stirred at room temperature until both reactants were completely dissolved. The resulting reaction mixture was placed in a Teflon-lined vessel and heated at 120 °C for 2 days. Upon returning the reaction vessel to room temperature, a pink crystalline product appeared on the bottom of the flask. The product was isolated by filtration and dried in vacuo. Yield: 1.0 g (∼71%). Anal. Calcd for **1** ($C_{28}H_{46}Co_2O_{25}$, MW: 900.51): C, 37.31; H, 5.11. Found: C, 37.50; H, 5.12%.

Transformation of $[Co_2(C_7H_{11}O_6)_4]_n \cdot nH_2O$ to $[Co(C_7H_{11}O_6)_2(H_2O)_2] \cdot 3H_2O$. $[Co_2(C_7H_{11}O_6)_4]_n \cdot nH_2O$ (0.25 g, 0.28 mmol) was dissolved in 4 mL of water. The reaction mixture was then stirred at room temperature and placed in the refrigerator at 4 °C. Addition of ethanol resulted in the precipitation of pink crystalline material on the bottom of the flask. The crystalline product was isolated by filtration and dried in vacuo. Yield: 0.12 g (40%). Positive identification of the product was achieved by FT-IR spectroscopy and X-ray crystallographic unit cell determination for one of the single crystals isolated.[35]

Transformation of $[Co(C_7H_{11}O_6)_2(H_2O)_2] \cdot 3H_2O$ to $[Co_2(C_7H_{11}O_6)_4]_n \cdot nH_2O$. $[Co(C_7H_{11}O_6)_2(H_2O)_2] \cdot 3H_2O$ (0.10 g, 0.19 mmol) was dissolved in 4 mL of water in a 25 mL round-bottom flask. The resulting mixture was then placed in a Teflon-lined vessel and heated at 120 °C for 2 days. Finally, a pink crystalline product appeared on the bottom of the vessel. The product was isolated by filtration and dried in vacuo. Yield: 0.060 g (71%). Positive identification of the product as **1** was achieved by FT-IR spectroscopy and X-ray crystallographic unit cell determination for one of the single crystals isolated.[35]

Synthesis of $[Zn_3(C_7H_{11}O_6)_6]_n \cdot nH_2O$ (2). The complex was prepared under hydrothermal conditions in a 23 mL Teflon-lined stainless steel container by heating a mixture of $Zn(CH_3COO)_2 \cdot 2H_2O$ (0.80 g, 3.6 mmol) and D-(−)-quinic acid (1.4 g, 7.3 mmol) in 10 mL of H_2O under continuous stirring. The pH of the resulting solution was ∼5. The mixture was heated at 160 °C for 72 h. The colorless crystals were isolated by filtration and dried in vacuo. Yield: 0.70 g (42%). Anal. Calcd for **2** ($C_{42}H_{68}O_{37}Zn_3$, MW: 1361.07): C, 37.03; H, 5.00. Found: C, 37.10; H, 4.96%.

X-Ray Crystal Structure Determination. Single crystals of **1** and **2** were obtained from aqueous solutions according to the described synthetic procedures. A single crystal with approximate dimensions 0.50 × 0.60 × 0.60 mm (**1**) and 0.50 × 0.35 × 0.30 mm (**2**) was mounted on a capillary. Diffraction measurements for **1** were taken on a Crystal Logic dual-goniometer diffractometer, using graphite monochromated Mo Kα radiation. Unit cell dimensions were determined and refined by using the angular settings of 25 automatically centered reflections in the range $11 < 2\theta < 23°$. Intensity data were recorded using $\theta-2\theta$ scans. Three standard reflections were monitored every 97 reflections over the course of data collection and showed less than 3% variation and no decay. Lorentz and polarization corrections were applied by using Crystal Logic software. Diffraction measurements for **2** were made on a Rigaku R-AXIS SPIDER Image Plate diffractometer using graphite monochromated Cu Kα radiation. Data collection (ω-scans) and processing (cell refinement, data reduction, and empirical absorption correction) were performed using the CrystalClear program package.[36] Important crystallographic data for both structures are listed in Table 1. Further experimental crystallographic details for **1**: $2\theta_{max} = 50°$; reflections collected/unique/used, 6016/5769 [$R_{int} = 0.0190$]/5769; 563 parameters refined; $\Delta/\sigma = 0.003$; $(\Delta\rho)_{max}/(\Delta\rho)_{min} = 0.300/-0.392$ e/Å^3; R/R_w (for all data), 0.0237/0.0634. For **2**, $2\theta_{max} = 65°$; reflections collected/unique/used, 32 836/7911 [$R_{int} = 0.1610$]/7911; 750 parameters refined; $(\Delta\rho)_{max}/(\Delta\rho)_{min} = 1.37/-0.92$ e/Å^3; R/R_w (for all data), 0.0679/0.1577.

The structures of **1** and **2** were solved by direct methods using SHELXS-97[37] and refined by full-matrix least-squares techniques on F^2 with SHELXL-97.[38] All hydrogen atoms in **1** and **2** were located by difference maps and were refined isotropically or were

(24) (a) Gran, G. *Acta Chem. Scand.* **1950**, *29*, 559–577. (b) Gran, G. *Analyst* **1952**, *77*, 661–671. (c) Rossotti, F. J. C.; Rossotti, H. *J. Chem. Educ.* **1965**, *42*, 375–378.
(25) Kong, L.-Y.; Zhu, H.-F.; Okamura, T.-A.; Mei, Y.-H.; Sun, W.-Y.; Ueyama, N. *J. Inorg. Biochem.* **2006**, *100*, 1272–1279.
(26) Pettit, L. D. *Molspin pH-meter Instruction Manual*; Molspin Ltd.: England.
(27) Irving, H. M.; Miles, M. G.; Petit, L. D. *Anal. Chim. Acta* **1967**, *38*, 475–479.
(28) Gans, P.; O'Sullivan, B. *Talanta* **2000**, *51*, 33–37.
(29) Harned, H. S.; Owen, B. B. *The Physical Chemistry of Electrolytic Solutions*, 3rd ed.; Reinhold Publishing Corp.: New York, 1958.
(30) Gans, P.; Sabatini, A.; Vacca, A. *J. Chem. Soc., Dalton Trans.* **1985**, 1195–1200.
(31) Zékány, L.; Nagypál, I.; Peintler, G. *PSEQUAD for Chemical Equilibria*; Technical Software Distributions: Baltimore, MD, 1991.
(32) Alderighi, L.; Gans, P.; Ienco, A.; Peters, D.; Sabatini, A.; Vacca, A. *Coord. Chem. Rev.* **1999**, *184*, 311–318.
(33) (a) Lacour, S.; Deluchat, V.; Bollinger, J.-C.; Serpaud, B. *Talanta* **1998**, *46*, 999–1009. (b) Reichle, R. A.; McCurdy, K. G.; Hepler, L. G. *Can. J. Chem.* **1975**, *53*, 3841–3845.
(34) Colston, B. J.; Robinson, V. J. *Analyst* **1997**, *122*, 1451–1455.
(35) Menelaou, M.; Konstantopai, A.; Mateescu, C.; Zhao, H.; Drouza, C.; Lalioti, N.; Salifoglou, A. *Inorg. Chem.* **2009**, *48*, 8092–8105.
(36) *CrystalClear*; Rigaku/MSC Inc.: The Woodlands, TX, 2005.
(37) Sheldrick, G. M. *SHELXS-97*; University of Göttingen: Göttingen, Germany, 1997.
(38) Sheldrick, G. M. *SHELXL-97*; University of Göttingen: Göttingen, Germany, 1997.

Table 1. Summary of Crystal, Intensity Collection, and Refinement Data for $[Co_2(C_7H_{11}O_6)_4]_n \cdot nH_2O$ (**1**) and $[Zn_3(C_7H_{11}O_6)_6]_n \cdot nH_2O$ (**2**)

	1	**2**
formula	$C_{28}H_{46}Co_2O_{25}$	$C_{42}H_{68}Zn_3O_{37}$
fw	900.51	1361.07
temp, K	298	298
wavelength	Mo Kα 0.71073	Cu Kα 1.54187
space group	$P2_1$	$P2_1$
a (Å)	5.768(3)	5.7095(1)
b (Å)	21.660(10)	32.3254(6)
c (Å)	13.150(7)	13.2471(2)
β (deg)	93.02(2)	93.036(1)
V (Å^3)	1640.6(14)	2441.48(7)
Z	2	2
D_{calcd}/D_{measd} (Mg m^{-3})	1.823/1.82	1.851/1.86
abs coeff (μ), mm^{-1}	1.119	2.780
	$-6 \le h \le 6$	$-6 \le h \le 5$
range of h, k, l	$-25 \le k \le 25$	$-38 \le k \le 38$
	$-0 \le l \le 15$	$-15 \le l \le 15$
goodness-of-fit on F^2	1.075	1.055
R^a	$R = 0.0236^b$	$R = 0.0658^b$
$R_w{}^a$	$R_w = 0.0633^b$	$R_w = 0.1568^b$

[a] R values are based on F values; R_w values are based on F^2. $R = \frac{\sum ||F_o| - |F_c||}{\sum (|F_o|)}$, $R_w = \sqrt{\sum [w(F_o^2 - F_c^2)^2] / \sum [w(F_o^2)^2]}$. [b] For 5735 (**1**), 7286 (**2**) reflections with $I > 2\sigma(I)$.

introduced at calculated positions as riding on bonded atoms. All non-hydrogen atoms in **1** and **2** were refined anisotropically.

Results

Syntheses. In an expedient synthetic procedure, Co(II) and D-(−)-quinic acid reacted in water:

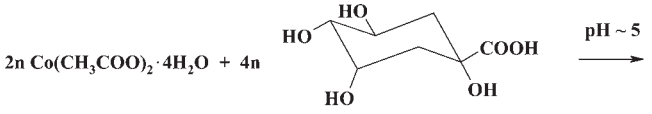

D-(-)-quinic acid Reaction 1

$$[Co_2(C_7H_{11}O_6)_4]_n \cdot nH_2O + 4n\,CH_3COOH + 7n\,H_2O$$

with a molar ratio of 1:2 at a pH of ~5 (reaction 1) under hydrothermal conditions. A similar procedure was carried out in the case of the binary system Zn(II) with D-(−)-quinic acid (reaction 2). The use of different bases was not crucial in the investigation of the two binary systems. On the contrary, the hydrothermal reaction conditions proved to be a significant factor assisting in the ultimate isolation of pure compounds **1** and **2**.

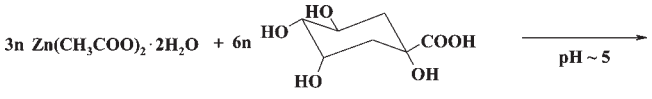

$$[Zn_3(C_7H_{11}O_6)_6]_n \cdot nH_2O + 6n\,CH_3COOH + 5n\,H_2O$$ Reaction 2

In the described synthetic approaches, the aforementioned simple reactions under hydrothermal conditions were very effective in providing pure crystalline materials suitable for further characterization through analytical, spectroscopic, and crystallographic studies. Elemental analyses on the derived products suggested the formulation $[Co_2(C_7H_{11}O_6)_4] \cdot H_2O$ for **1** and $[Zn_3(C_7H_{11}O_6)_6] \cdot H_2O$ for **2**. Further X-ray crystallographic investigations confirmed the above analytical formulations.

Compounds **1** and **2** are stable in the air for long periods of time. Compound **1** is soluble in water unlike compound **2**, and both crystalline materials are insoluble in organic solvents, acetonitrile, chlorinated solvents ($CHCl_3$, CH_2Cl_2), toluene, and DMF.

Co(II)-(D-(−)-Quinic Acid) Transformation Chemistry. Poised to understand the association between two different species arising from the same binary system Co(II)-(D-(−)-quinic acid), the potential synthetic link between compound **1** and the mononuclear compound $[Co(C_7H_{11}O_6)_2(H_2O)_2] \cdot 3H_2O$[35] was explored. To this end, compound **1** was dissolved in water and placed in the refrigerator at 4 °C (Scheme 1). The addition of ethanol as a precipitating agent afforded a pink crystalline material identified as $[Co(C_7H_{11}O_6)_2(H_2O)_2] \cdot 3H_2O$[35] by (a) FT-IR spectroscopy and (b) X-ray crystallographic determination of the cell parameters of a single crystal from the isolated crystalline material. Through this approach, **1** was linked to well-defined species arising from the same binary system.

In an analogous fashion, compound $[Co(C_7H_{11}O_6)_2(H_2O)_2] \cdot 3H_2O$ was dissolved in water and, under specific hydrothermal conditions, afforded pink crystals. The crystalline material, characterized through FT-IR spectroscopy and X-ray crystal structure determination of the cell parameters, was proven to be identical to **1**. Finally, the mononuclear compound was proven to be the dominant species in the aqueous Co(II)−(D-(−)-quinate) system, as it is involved in several interwoven transformations, encompassing the mononuclear species $[Co(C_7H_{11}O_6)_2]^0$ and the associated mononuclear species containing Co(II) bound to three molecules of D-(−)-quinic acid $[Co(C_7H_{11}O_6)_3]^-$ (Scheme 1).[35]

X-Ray Crystallographic Structures. The three-dimensional X-ray crystal structure determination of complexes **1** and **2** revealed the formation of 2D polymeric structures. Complex **1** crystallizes in the monoclinic space group $P2_1$. The DIAMOND diagram of the organic−inorganic hybrid $[Co_2(C_7H_{11}O_6)_4]_n \cdot nH_2O$ is shown in Figure 1. A select list of interatomic bond distances and angles for **1** is given in Table 2. In the observed 2D molecular lattice of polymeric compound **1**, the repeating unit consists of discrete dinuclear $[Co_2(C_7H_{11}O_6)_4]^0$ entities. A water molecule of solvation completes the crystallographic molecular formulation. In each such dinuclear unit, there are two six-coordinate and symmetry-independent Co(II) ions interacting with four quinate ligands each. The first type of Co(II) ions, dubbed the Co(1) assembly, involves four carboxylato and two alcoholic oxygen atoms from four different quinate ligands. Specifically, one quinate ligand coordinates to the metal ion through the carboxylate and alcoholic oxygens O(1) and O(3), respectively. These two moieties bind the Co(II) ion, promoting the formation of a five-membered metallacyclic ring and rendering the arising species quite stable. The D-(−)-quinic acid is singly deprotonated through the carboxylic acid binding site, with the α-hydroxy group retaining its proton. The formation of the five-membered metallacyclic ring has already been shown to be present in other Co(II)−quinate species that have been both isolated and well-characterized.[35] The second carboxylate oxygen atom of that quinate ligand, O(2), is coordinated to a neighboring Co(1)‴ ion (‴ = $-1 + x, y, z$), leading

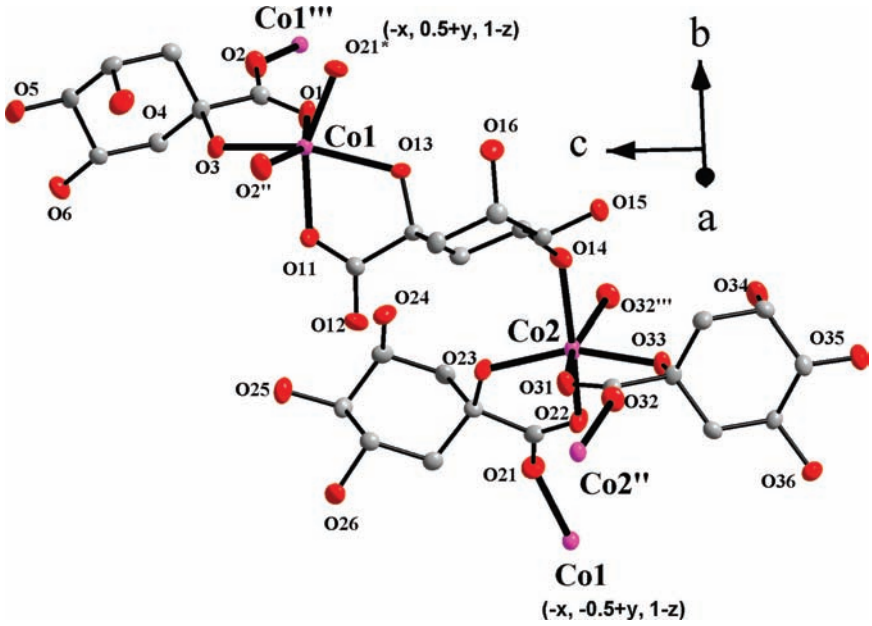

Figure 1. Crystal structure of the repeating unit in $[Co_2(C_7H_{11}O_6)_4]_n \cdot nH_2O$ (**1**). Thermal ellipsoids are drawn by DIAMOND and represent 30% probability surfaces. Hydrogen atoms have been omitted for clarity. Primed atoms are generated by symmetry operations: (′) $-x, 0.5 + y, 1 - z$; (″) $1 + x, y, z$; (‴) $-1 + x, y, z$.

Scheme 1. Transformation Chemistry of the Binary System Co(II)−D-(−)-Quinic Acid

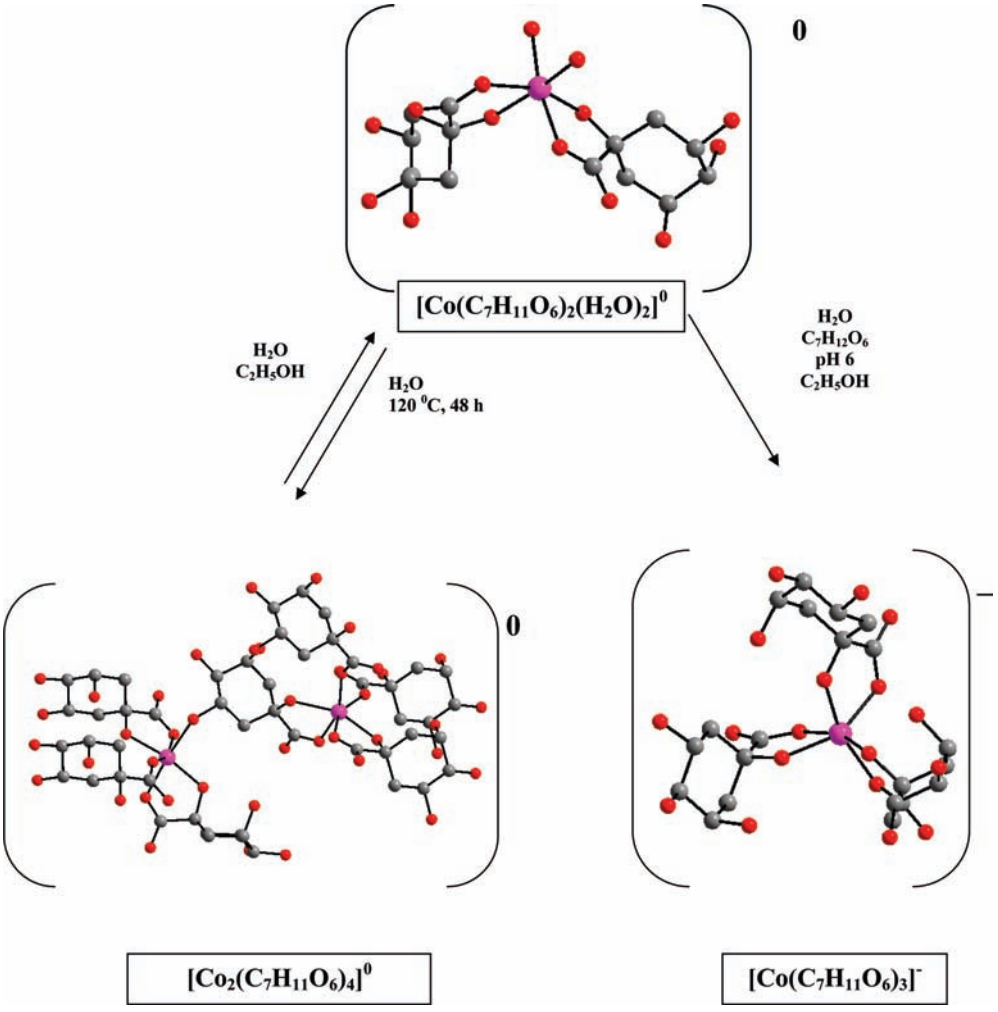

to a *syn*−*anti* bridging mode of the carboxylate moiety. The aforementioned mode of coordination is shown in Scheme 2 (mode I). The distance between the Co(II) ions [Co(1) and Co(1)‴] is equal to the length of the

Table 2. Bond Lengths [Å] and Angles [deg] in **1**[a]

distances			
Co(1)−O(21)′	2.014(2)	Co(2)−O(32)‴	2.037(2)
Co(1)−O(11)	2.067(2)	Co(2)−O(31)	2.056(2)
Co(1)−O(2)″	2.086(2)	Co(2)−O(22)	2.069(2)
Co(1)−O(3)	2.089(2)	Co(2)−O(23)	2.107(2)
Co(1)−O(1)	2.104(2)	Co(2)−O(33)	2.109(2)
Co(1)−O(13)	2.213(2)	Co(2)−O(14)	2.267(2)
angles			
O(11)−Co(1)−O(2)″	88.9(1)	O(31)−Co(2)−O(22)	107.5(1)
O(2)″−Co(1)−O(3)	79.0(1)	O(31)−Co(2)−O(23)	92.5(1)
O(21)′−Co(1)−O(1)	90.6(1)	O(32)‴−Co(2)−O(33)	85.1(1)
O(3)−Co(1)−O(1)	74.9(1)	O(22)−Co(2)−O(33)	89.2(1)
O(21)′−Co(1)−O(13)	83.2(1)	O(32)‴−Co(2)−O(14)	79.7(1)
O(11)−Co(1)−O(13)	73.1(1)	O(23)−Co(2)−O(14)	99.9(1)

[a] Symmetry transformations used to generate equivalent atoms: (′) $-x, 0.5 + y, 1 - z$; (″) $1 + x, y, z$; (‴) $-1 + x, y, z$.

crystallographic *a* axis (5.768(3) Å). Therefore, this type of bridging leads to the formation of chains of Co(1) assemblies along the *a* axis. Moreover, a second quinate ligand is coordinated to the Co(1) ion in a similar coordination mode through one of its alcoholic and carboxylate oxygen atoms, O(13) and O(11), respectively. However, the second terminal carboxylate oxygen O(12) does not participate in the coordination sphere of the Co(1) ion. Thus, the carboxylate group of the second quinate ligand employed adopts a monodentate coordination mode, as is depicted in Scheme 2 (mode II). The remaining alcoholic groups of the D-(−)-quinate ligand remain protonated. Therefore, each quinate Co(II) binder is singly deprotonated though the carboxylic binding site. The coordination sphere of Co(1) is filled through participation, at terminal positions, of two carboxylate oxygen atoms, O(2)″ (″ = 1+*x*, *y*, *z*) and O(21)* (* = $-x$, $0.5 + y$, $1 - z$), which belong to quinate ligands that bind Co(1) centers along the crystallographic *a* axis and link Co(1) with Co(2) centers along the crystallographic *b* axis.

The second type of Co(II) centers, reflected as Co(2) in complex **1**, exhibit a different coordination sphere from that in Co(1) centers. In particular, four coordination sites are occupied by two different quinate ligands, where both bind the aforementioned cobalt ion through the (a) α-alcoholic oxygens O(23) and O(33) and (b) carboxylate oxygens O(22) and O(31). The oxygen atoms O(31) and O(33) and O(22) and O(23) promote the formation of two five-membered metallacyclic rings around Co(2) centers, as was observed for Co(1) centers. Another coordination site is occupied by the oxygen terminal O(32)‴ [(‴) = $-1 + x, y, z$] of the carboxylic binding site of an abutting quinate ligand attached to a nearby cobalt ion Co(2)″ [(″) = $1 + x, y, z$]. The distance of Co(2)···Co(2)″ is equal to 5.768(3) Å, i.e., the length of the crystallographic *a* axis. As a result, polymeric chains of the Co(2) assemblies are formed, parallel to the crystallographic *a* axis. The Co(2)···Co(2)″ chains together with the Co(1)···Co(1)‴ chains mentioned above form a polymeric chain of $[Co_2(C_7H_{11}O_6)_4]^0$ dimers along the crystallographic *a* axis. The remaining coordination site of Co(2) ion is occupied by an oxygen atom originating in one of the three protonated alcoholic moieties O(14) of a quinate ligand, which through its other termini (O(11) and O(13) atoms) is anchored to the first discrete Co(1) ion described above. In this respect, the coordination sphere of Co(2) differs from that of Co(1). Even though the coordination number of Co(2) is six, three carboxylato and three alcoholic oxygen atoms from four different quinate ligands are involved, with the arising coordination environment being distorted octahedral. The equatorial plane of the octahedron is formulated by the oxygen terminals O(22), O(32)‴, O(31), and O(14), while the alcoholic oxygens O(23) and O(33) fulfill the axial requirements of the Co(2) environment. The $[Co_2(C_7H_{11}O_6)_4]_n$ chains of dimers, developed parallel to the crystallographic *a* axis, are repeated along the crystallographic *b* axis through the 2-fold screw axis that runs parallel to it and passes through point (0, 0, 0.5) (Figure 2a). Along the *b* axis, dimer chains are linked through carboxylic O(21) oxygen atom of the corresponding quinate ligand, forming a 2D polymer parallel to the (0, 0, 1) crystallographic plane.

Scheme 2

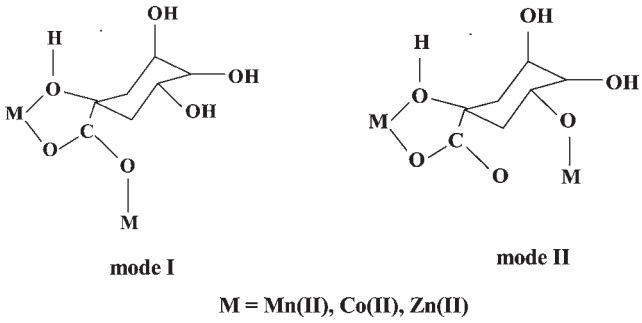

M = Mn(II), Co(II), Zn(II)

In conclusion, several things are responsible for the formation of the 2D polymeric structure (Figure 2b) of compound **1**: (a) the multifunctional nature of the crystallographically distinct Co(II)-interacting quinate ligands, (b) the way the quinates extend into the coordination sphere of Co(II) ions, promoting various coordination modes, and (c) hydrogen-bonding interactions (vide infra).

Complex **2** crystallizes in the monoclinic space group $P2_1$. The DIAMOND diagram of the repeating unit in $[Zn_3(C_7H_{11}O_6)_6]_n \cdot nH_2O$ is shown in Figure 3. A select list of interatomic bond distances and angles for **2** is given in Table 3. The 2D polymeric structure of complex **2** is built by the repetition of discrete $[Zn_3(C_7H_{11}O_6)_6]$ trinuclear units formed by three symmetry-independent Zn atoms and six symmetry-independent quinic ligands. A water molecule of solvation completes the crystallographic molecular formulation. The coordination sphere of each Zn(II) ion is filled by six oxygen atoms. In each triad formed, the metal−quinate assembly forms differently from the coordination point of view. Specifically, each Zn(II) ion of every triad involves four quinate ligands, yet the formation of the assembly in Zn(1) is different compared to those in Zn(2) and Zn(3), which share a similar coordination status. In addition, three carboxyl oxygens [O(1), O(2), and O(12)] are coordinated to Zn(1) originating in three different quinate ligands. Two of the carboxylate oxygens, namely, O(1) and O(12), participate in the formation of two five-membered cyclic rings involving the alcoholic oxygens O(3) and O(13), respectively. Therefore, each quinate ligand acts as a bidentate ligand, being singly deprotonated, with

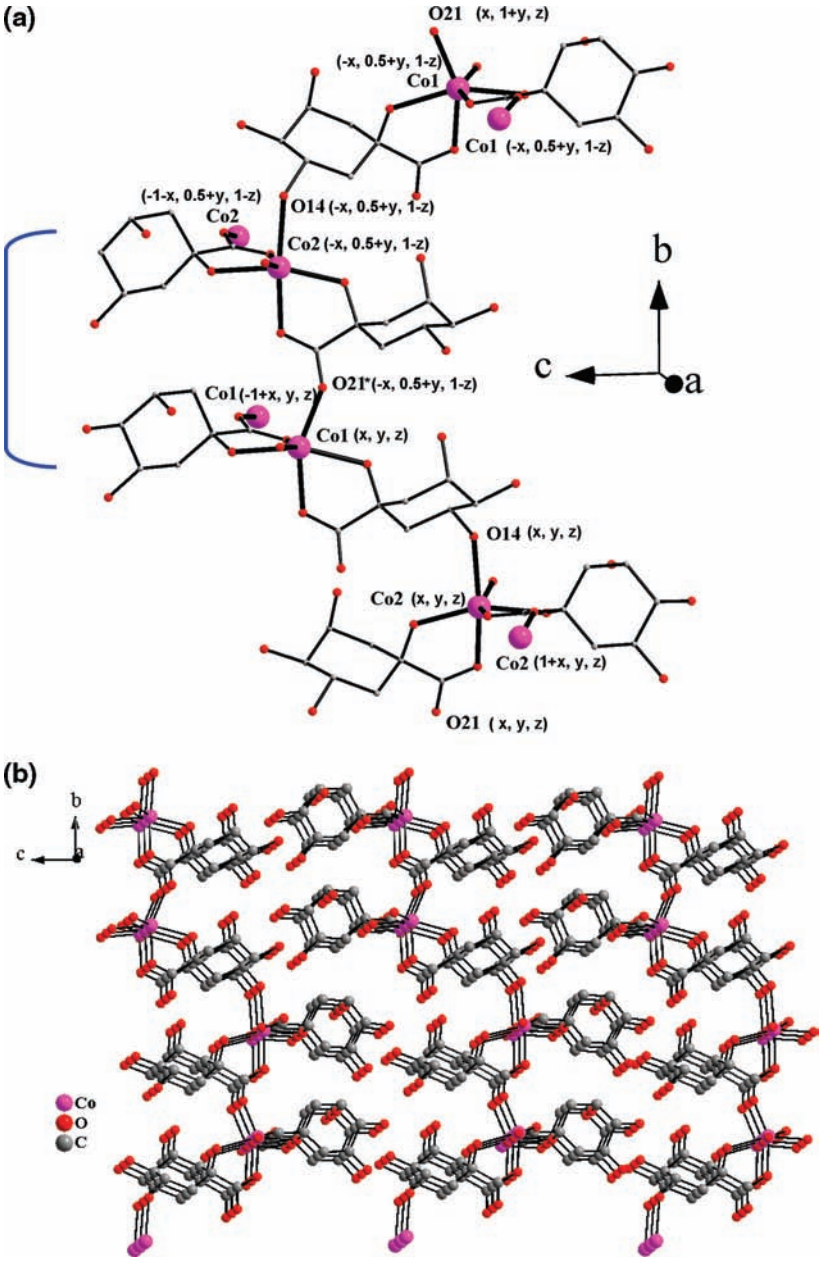

Figure 2. (a) Link of $[Co_2(C_7H_{11}O_6)_4]$ dimers along the 2-fold screw axis [2 (0, 1/2, 0) (0, *y*, 0.5)]. The bracket in the left indicates the repeating unit of dimers. Next to each selected atom is given the symmetry operation that brings that atom at the specific position. (b) Packing diagram of **1** in the *bc* plane.

the deprotonated site being the carboxylate group. The α-hydroxy groups involved remain protonated, and as such they coordinate to the metal ion center. The fifth coordination site of Zn(1) is occupied by another carboxyl oxygen O(2) belonging to a different quinate binder. The last coordination site of the six coordinate octahedral geometry of Zn(1) is filled through an alcoholic oxygen [O(56)*] from a fourth quinate ligand involved. The formation of the coordination sphere of Zn(2) and Zn(3) is similar. In particular, in both Zn(II) ions left to complete the triad, two five-membered metallacyclic rings form through the carboxylate oxygens [O(21) and O(32) and O(41) and O(51), respectively] and the α-alcoholic oxygens [O(23) and O(33) and O(43) and O(52), respectively]. Therefore, the quinate ligands act as bidentate ligands, and the deprotonated site in each quinate ligand is the carboxylate group, much like in the case of Zn(1). The two remaining sites of Zn(2) and Zn(3) are occupied by carboxylate oxygens [O(22) and O(11) and O(31) and O(42), respectively] from two different quinate ligands for each ion. Zn(1), Zn(2), and Zn(3) atoms are bridged to three Zn(1)′, Zn(2)′, and Zn(3)′ atoms (′ = 1 + *x*, *y*, *z*), respectively, translated along the crystallographic *a* axis, with the help of three quinic ligands binding through their carboxylate oxygen atoms O(2), O(22), and O(42). The result is the formation of chains of trimers along the crystallographic *a* axis. The $[Zn_3(C_7H_{11}O_6)_6]$ chains of trimers that develop parallel to the crystallographic *a* axis are repeated along the crystallographic *b* axis through the 2-fold screw axis that runs parallel to it and passes through point (0.5, 0, 0.5). Along the crystallographic *b* axis, the chains of trimers are linked through carboxylic oxygen atom O(56) of the corresponding quinate ligand, forming a 2D polymer parallel

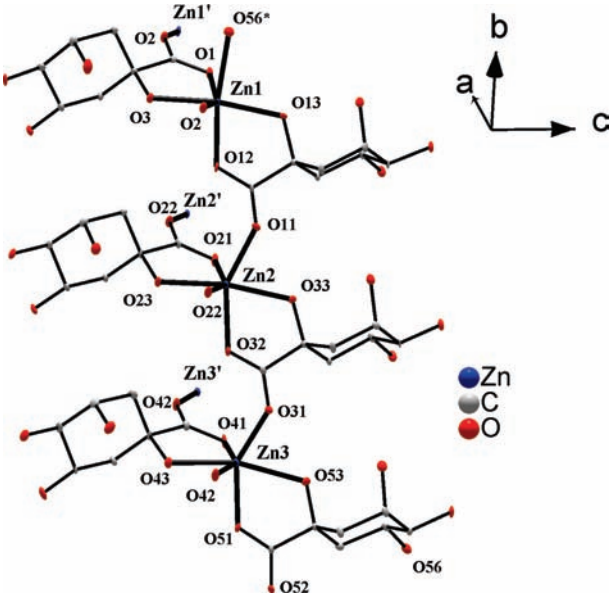

Figure 3. Crystal structure of the repeating unit in $[Zn_3(C_7H_{11}O_6)_6]_n \cdot nH_2O$ (**2**). Thermal ellipsoids are drawn at 40% probability surfaces. Primed atoms are generated by the symmetry operations (′) $1 + x, y, z$ and (′) $x, 1 + y, z$. Atoms with stars are generated by the symmetry operation (∗) $1 - x, 0.5 + y, 1 - z$. Atoms with primes and stars are generated by the symmetry operation (′*) $-x, 0.5 + y, 1 - z$.

Table 3. Bond Lengths [Å] and Angles [deg] in **2**[a]

distances			
Zn(1)−O(12)	2.027(4)	Zn(2)−O(11)	2.084(4)
Zn(1)−O(2)′	2.029(4)	Zn(2)−O(23)	2.118(4)
Zn(1)−O(1)	2.031(4)	Zn(2)−O(33)	2.152(4)
Zn(1)−O(3)	2.109(4)	Zn(3)−O(31)	1.983(4)
Zn(1)−O(13)	2.124(4)	Zn(3)−O(51)	2.044(4)
Zn(1)−O(56)″	2.350(4)	Zn(3)−O(41)	2.067(4)
Zn(2)−O(32)	2.065(4)	Zn(3)−O(42)′	2.082(4)
Zn(2)−O(22)′	2.075(4)	Zn(3)−O(43)	2.124(4)
Zn(2)−O(21)	2.080(4)	Zn(3)−O(53)	2.329(4)
angles			
O(12)−Zn(1)−O(2)′	90.9(2)	O(21)−Zn(2)−O(23)	75.2(2)
O(2)′−Zn(1)−O(3)	83.7(2)	O(32)−Zn(2)−O(33)	75.0(2)
O(1)−Zn(1)−O(3)	76.6(2)	O(11)−Zn(2)−O(33)	78.5(2)
O(12)−Zn(1)−O(13)	77.2(1)	O(31)−Zn(3)−O(41)	93.1(2)
O(1)−Zn(1)−O(56)″	85.2(2)	O(51)−Zn(3)−O(42)′	89.6(2)
O(13)−Zn(1)−O(56)″	95.8(2)	O(41)−Zn(3)−O(43)	74.9(2)
O(21)−Zn(2)−O(11)	87.5(2)	O(42)′−Zn(3)−O(43)	76.4(2)
O(22)′−Zn(2)−O(23)	79.8(2)	O(31)−Zn(3)−O(53)	78.9(2)
O(22)′−Zn(2)−O(32)	88.4(2)	O(51)−Zn(3)−O(53)	71.2(2)

[a] Symmetry transformations used to generate equivalent atoms: (′) $x - 1, y, z$; (″) $-x + 1, y + 1/2, 1 - z$.

to the (0, 0, 1) crystallographic plane. The development of the chain of abutting Zn(II) trimers extending along the crystallographic *b* axis is shown in Figure 4.

The molecular structures of **1** and **2** are further stabilized through an extensive network of intra- and intermolecular hydrogen bonding interactions (see the Supporting Information). The intermolecular hydrogen bonding interactions emerge along the crystallographic *c* axis and generate an overall 3D framework structure.

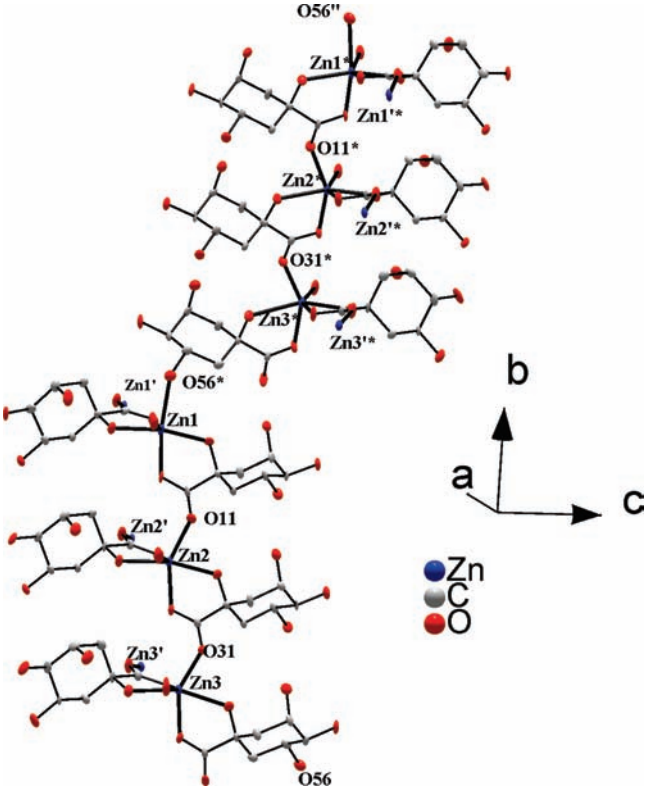

Figure 4. Development of the chain of trimers of **2** along the 2-fold screw axis [2 (0, 1/2, 0) (0.5, *y*, 0.5)]. Primed atoms are generated by the symmetry operation (′) $1 + x, y, z$. Atoms with stars are generated by the symmetry operation (∗) $1 - x, 0.5 + y, 1 - z$.

Representative examples of complexes between divalent metal ions such as Mn(II), Cu(II), and Ni(II) and carboxylate-bearing substrates include the citrate-containing complexes $(NH_4)_4[Mn^{II}(C_6H_5O_7)_2]$ (**3**),[39] $[Cd^{II}(C_6H_6O_7)(H_2O)]_n$ (**4**),[40] $(NH_4)_4[Cu^{II}(C_6H_5O_7)_2]$ (**5**),[41] $K_2[Ni^{II}(C_6H_5O_7)(H_2O)_2]_2 \cdot 4H_2O$ (**6**),[42] and $[Pb^{II}(C_6H_6O_7)]_n \cdot nH_2O$ (**7**).[43]

The Co−O bond distances are in the range from 2.014(2) to 2.267(2) Å found in **1**, and they are of comparable length with those found in $[Co^{II}\{(CH_3)_3NCH_2COO\}_2(H_2O)_4]Cl_2 \cdot 4H_2O$ (2.087(2)−2.101(2) Å),[44] $[Co^{II}(C_2H_5OH)_6][CoBr_4]$ (2.01(3)−2.14(3) Å),[45] and $[Co^{II}(COO-CH_2-CHOH-COO)] \cdot 3H_2O$ (2.067(3)−2.136(3) Å).[46] The octahedral cobalt ion in **1** exhibits similarities with other octahedral divalent metal ions, such as Zn(II)[47] and Ni(II)[48] in analogous octahedral species. The M−O distances observed in those complexes are in line with those seen in **1** and range from 2.052(2) to 2.164(2) Å (Zn(II)) and 2.021(3) to 2.072(3) Å

(39) Matzapetakis, M.; Karligiano, N.; Bino, A.; Dakanali, M.; Raptopoulou, C. P.; Tangoulis, V.; Terzis, A.; Giapintzakis, J.; Salifoglou, A. *Inorg. Chem.* **2000**, *39*, 4044–4051.

(40) Dakanali, M.; Kefalas, E. T.; Raptopoulou, C. P.; Terzis, A.; Mavromoustakos, T.; Salifoglou, A. *Inorg. Chem.* **2003**, *42*, 2531–2537.

(41) Bott, R. C.; Sagatys, D. S.; Lynch, D. E.; Smith, G.; Kennard, C. H. L.; Mak, T. C. W. *Aust. J. Chem.* **1991**, *44*, 1495–1498.

(42) Baker, E. N.; Baker, H. M.; Anderson, B. F.; Reeves, R. D. *Inorg. Chim. Acta* **1983**, *78*, 281–285.

(43) Kourgiantakis, M.; Matzapetakis, M.; Raptopoulou, C. P.; Terzis, A.; Salifoglou, A. *Inorg. Chim. Acta* **2000**, *297*, 134–138.

(44) Chen, X.-M.; Mak, T. C. W. *Acta Crystallogr.* **1992**, *C48*, 1211–1214.

(45) Bkouche-Waksman, I.; L'Haridon, P. *Bull. Soc. Chim. Fr.* **1979**, *1−2*, I50–I53.

(46) Kryger, L.; Rasmussen, S. E. *Acta Chem. Scand.* **1972**, *26*, 2349–2359.

(47) Zevaco, T. A.; Görls, Z.; Dinjus, E. *Inorg. Chim. Acta* **1998**, *269*, 283–286.

(48) Zhou, Z.-H.; Lin, Y.-J.; Zhang, H.-B.; Lin, G.-D.; Tsai, K.-R. *J. Coord. Chem.* **1997**, *42*, 131–141.

(Ni(II)), while a wider range due to Jahn−Teller distortion is observed in the copper analog (1.969(3)−2.341(3) Å).

The Zn−O bond distances are in the range from 2.027(4) to 2.350(4) Å [Zn(1)−O], 2.065(4) to 2.152(4) Å [Zn(2)−O], and 1.983(4) to 2.329(4) Å [Zn(3)−O] found in **2**, and they are in good agreement with the bond distances found in $[Zn_3(C_6H_5O_7)_2(H_2O)_2]_n$,[49] $(NH_4)_4[Zn(C_6H_5O_7)_2]$,[50] $[Zn(C_4H_4O_5)(C_{10}H_8N_2)\cdot 3H_2O]_n$,[51] $[Zn(C_3H_5O_3)_2(C_3H_4N_2)_2]\cdot 0.5H_2O$, and $[Zn(C_4H_7O_3)_2(C_3H_4N_2)_2]$.[52]

Finally, compound **1** is isostructural with the metal−organic hybrid $[Mn_2(C_7H_{11}O_6)_4]_n\cdot nH_2O$.[53] Also comparable are the M−O distances occurring in various quinate complexes such as $K[Co(C_7H_{11}O_6)_3]\cdot 3CH_3CH_2OH$,[35] $Na[Co(C_7H_{11}O_6)_3]\cdot 3CH_3CH_2OH\cdot 2.25H_2O$, $[Co(C_7H_{11}O_6)_2(H_2O)_2]\cdot 3H_2O$, $Na[Ni(C_7H_{11}O_6)_3]\cdot 2.75H_2O$,[54] $[Cu(C_7H_{10}O_6)(H_2O)]_2(H_2O)_2$,[55] $\{[Cu(NO_3)(C_7H_{11}O_6)(H_2O)]\cdot 2H_2O\}_n$, $\{[CuCl(C_7H_{11}O_6)(H_2O)]\cdot H_2O\}_n$,[56] $[Pt(C_6H_{14}N_2)(C_7H_{10}O_6)]$,[57] $[Zn(C_7H_{11}O_6)_2]$,[58] $[Cd(C_7H_{11}O_6)_2]\cdot H_2O$, and $(NH_4)_2\{[V(O)_2]_2[V(O)](\mu\text{-}C_7H_{10}O_6)_2\}\cdot H_2O$.[59]

Overall, the quinate ligand is proven to play the role of an efficient metal ion chelator, employing various types of anchors (mode I and mode II in Scheme 2) due to its multifunctional chemical structure and its effective coordination ability in formulating the coordination environment around divalent metal ions, such as Mn(II), Co(II), and Zn(II).

Electronic Spectroscopy. The UV/visible spectrum of **1** was taken in water (see the Supporting Information). The spectrum shows a well-defined major peak at λ_{max} = 512 nm (ε = 13 M^{-1} cm^{-1}), with a shoulder-like band around λ = 476 nm ($\varepsilon \sim 10$ M^{-1} cm^{-1}). In addition, a distant band rising into the UV region appears at 287 nm (ε 800 M^{-1} cm^{-1}). The absorption features in the low energy region are most likely due to d−d transitions, which are typical for a Co(II) d^7 octahedral species.[60] The multiply structured band around 512 nm could be tentatively attributed to the $^4T_{1g} \rightarrow {}^4T_{1g}(P)$ transition. The observed multiple structure is in good agreement with literature reports invoking (a) the admixture of spin forbidden transitions to doublet states derived from ^2G and ^2H, (b) spin−orbit coupling, and (c) vibrational or low symmetry components, to account for the complexity of the spectrum.[61] The UV−visible spectrum of **1** in water is different from that of $Co(II)_{aq}$,[62] reflecting the unique coordination sphere composition of Co(II) in solution.

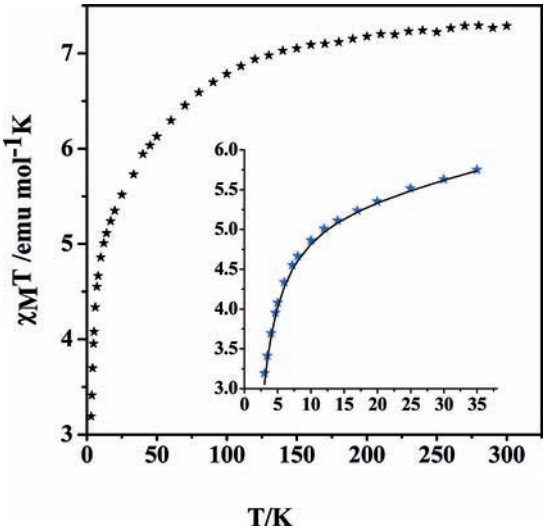

Figure 5. Temperature dependence of the magnetic susceptibility of **1**, in the form of $\chi_M T$ vs T, in the temperature range 3.0−290.0 K using an external magnetic field of 0.5 T. The solid line represents the fitting results (see text).

Infrared Spectroscopy. The FT-infrared spectra of **1** and **2** in KBr revealed the presence of resonances attributed to vibrationally active carbonyls of the quinate ligand. In both **1** and **2**, the antisymmetric stretching vibrations $\nu_{as}(COO^-)$ appear between 1639 and 1607 cm^{-1} for **1** and 1654 and 1597 cm^{-1} for **2**. The aforementioned bands likely overlap with scissoring vibrations of water. The symmetric stretching vibrations $\nu_s(COO^-)$ appear between 1451 and 1380 cm^{-1} for **1** and 1421 and 1416 cm^{-1} for **2**. Quinate CH_2 wagging vibrations likely coexist in the same region. Both water and/or quinate methylene group vibrations in the same frequency regions of the spectrum as those of the carboxylate groups in the metal-bound quinate ligand do not hamper interpretation of the spectra. In **1** and **2**, the frequencies of the bands of the antisymmetric and symmetric stretching vibrations are shifted to lower values compared to the corresponding vibrations in free D-(−)-quinic acid, thus indicating a change in the coordination status of the carboxylates in the quinate ligand. The frequency difference, $\Delta(\nu_{as}(COO^-) - \nu_s(COO^-))$,[63,64] in both **1** and **2** is greater than 200 cm^{-1}, indicating the presence of deprotonated carboxylate groups coordinated to the metal ions in a monodentate fashion. This contention is further proven by the X-ray crystal structure determination of **1** and **2**.

Magnetic Susceptibility. Magnetic susceptibility measurements on complex **1** were carried out at different magnetic fields and in the temperature range 3.0−290.0 K. Figure 5 shows the $\chi_M T$ versus T magnetic susceptibility data at 0.5 T. The $\chi_M T$ values decrease from

(49) Zhang, G.; Yang, G.; Ma, J. S. *Cryst. Growth Des.* **2006**, *6*, 371–381.
(50) Swanson, R.; Ilsley, W. H.; Stanislowski, A. G. *J. Inorg. Biochem.* **1983**, *18*, 187–194.
(51) Yi-Shan Song, Y. S.; Yan, B.; Chen, Z. X. *J. Sol. State Chem.* **2006**, *179*, 4037–4046.
(52) Carballo, R.; Castineiras, A.; Covelo, B.; Garcia-Martinez, E.; Niclos, J.; Vazquez-Lopez, E. M. *Polyhedron* **2004**, *23*, 1505–1518.
(53) Menelaou, M.; Raptopoulou, C. P.; Terzis, A.; Tangoulis, V.; Salifoglou, A. *Eur. J. Inorg. Chem.* **2005**, *10*, 1957–1967.
(54) Menelaou, M.; Mateescu, C.; Zhao, H.; Lalioti, N.; Salifoglou, A. *Polyhedron* **2009**, *28*, 883–890.
(55) Barba-Behrens, N.; Salazar-Garcia, F.; Bello-Ramirez, A. M.; Garcia-Baez, E.; Rosales-Hoz, M. J.; Contreras, R.; Flores-Parra, A. *Trans. Met. Chem.* **1994**, *19*, 575–581.
(56) Bkouche-Walksman, I. *Acta Crystallogr., Sect. C* **1994**, *50*, 62–64.
(57) Hata, G.; Kitano, Y.; Kaneko, T.; Kawai, H.; Mutoh, M. *Chem. Pharm. Bull.* **1992**, *40*, 1604–1605.
(58) Inomata, Y.; Haneda, T.; Howell, F. S. *J. Inorg. Biochem.* **1999**, *76*, 13–17.
(59) Codd, R.; Hambley, T. W.; Lay, P. A. *Inorg. Chem.* **1995**, *34*, 877–882.
(60) Drago, R. S. *Physical Methods in Chemistry*; W. B. Saunders Company: Philadelphia, 1977.
(61) Lever, A. B. P. *Inorganic Electronic Spectroscopy*, 2nd ed.; Elsevier: Amsterdam, 1984.
(62) (a) Figgis, B. N. *Introduction to Ligand Fields*; Interscience Publishers: New York, 1966. (b) Jorgensen, C. K. *Adv. Chem. Phys.* **1963**, *5*, 33–146. (c) Ballhausen, C. J. *Introduction to Ligand Field Theory*; McGraw-Hill Book Co.: New York, 1962.
(63) Djordjevic, C.; Lee, M.; Sinn, E. *Inorg. Chem.* **1989**, *28*, 719–723.
(64) Deacon, G. B.; Philips, R. J. *Coord. Chem. Rev.* **1980**, *33*, 227–250.

7.2 emu mol^{-1} K at 290 K to 3.2 emu mol^{-1} K at 3.0 K. The high-temperature value of $\chi_M T$ is higher than 3.75 emu mol^{-1} K, the value that would be expected for a Co(II) dinuclear system with $S_1 = S_2 = 3/2$ ($g = 2$).

This behavior is consistent with the presence of a significant orbital contribution to the anisotropic nature of the Co(II) system investigated. Co(II) can be described by the low-lying spin-doublet $S = 1/2$, which is anisotropic in Co(II). It must be pointed out that in Co(II) this effective spin doublet arises from the splitting of the $^4T_1$ term through spin−orbit coupling and local distortion of the octahedral sites. To verify the magnitude of the exchange interaction in **1**, if any, the general quantum mechanical operator can be written explicitly as

$$H = -(J_z S_1^z S_2^z + J_x S_1^x S_2^x + J_y S_1^y S_2^y) + B \cdot g_i \cdot S_i \qquad (1)$$

where $i = 1$ and 2, the effective spin is $S_1 = S_2 = 1/2$, and axial J ($J_x = J_y$, J_z) and g ($g_x = g_y$, g_z) values are considered. This anisotropic model limits its applicability in the low-temperature range ($T < 30$ K).[65,66] There, only the lowest lying spin doublet of Co(II) is significantly populated, yet that is adequate to obtain useful information on the exchange parameter J. When $J_z \neq 0$ and $J_x = J_y = 0$, the system is in the Ising limit. When $J_z = 0$ and $J_x = J_y \neq 0$, the system is in the XY limit.

The best fit of the experimental susceptibility data to the expression of the magnetic susceptibility derived from this model gives an exchange parameter $J_z = -2.1(2)$ cm^{-1}, $g_z = 7.2(2)$, $J_{xy}/J_z = 0.37(2)$, and $g_{xy}/g_z = 0.57(2)$ and is shown as a solid line in the inset of Figure 5. Bearing in mind that $J_{iso} = (J_x + J_y + J_z)/3$, the value of the isotropic exchange constant J_{iso} for this model is $J_{iso} = -1.21(2)$ cm^{-1}, which is in accordance with a small anisotropic antiferromagnetic interaction.

To test the validity of the fitting values, the magnitude of the anisotropy for the Co−Co interaction was investigated. Generally, that is given by $J_{xy}/J_z \sim (g_{xy}/g_z)^2$, where J_{xy} and J_z are the parallel and perpendicular exchange components, respectively, to the spin direction (J has been assumed to be axial).[66,67] On the basis of the values obtained from the fitting process, an agreement arises between the two terms of the aforementioned mathematical relationship.

Magnetization Studies. Magnetization measurements on **1** were run at three different temperatures (2.5, 3, and 4 K), and in the field range 0−7 T. The derived data are shown in the form of $M/N\mu_B$ vs H/T in Figure 6. The large value of $M_{saturation}$ (5 μ_B at 2.5 K) is in accordance with a very small interaction between the two Co(II) magnetic centers. To further investigate the fitting process, simulations of the magnetization data (vide infra) were carried out at different temperatures using the values obtained from the susceptibility fitting. The results are shown also in Figure 6 as solid lines. Here, too, the observed simulations are in agreement with the experimental curves.

EPR Spectroscopy. To explore the existence of a weak interaction between the Co(II) centers in complex **1**,

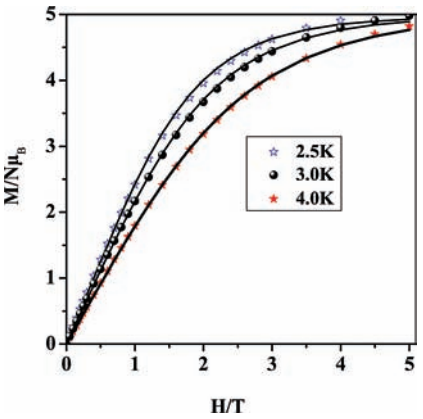

Figure 6. Magnetization of **1**, in the form of $M/N\mu_B$ vs H/T, at 2.5, 3.0, and 4.0 K and in the field range 0−7 T. Fitting results are shown as solid lines.

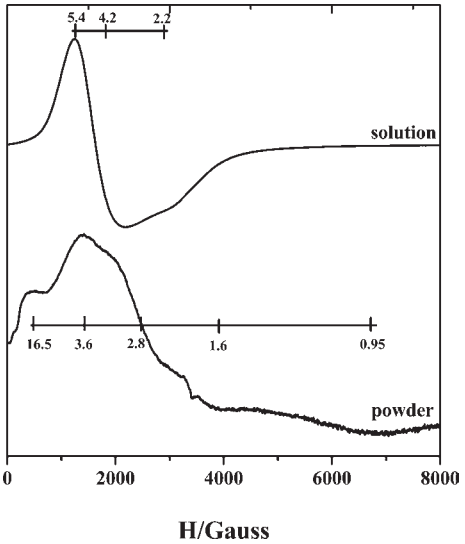

Figure 7. Powder X-band EPR spectrum of **1** in the field range 0−8000 G. Frozen water solution X-band EPR spectrum in the field range 0−8000 G.

X-band powder and solution EPR experiments were carried out in the temperature range 4−40 K (Figure 7). As a consequence of the fast spin−lattice relaxation time of high-spin Co(II), signals were observed only below 40 K. The g values obtained from the powder EPR spectrum show large variations in the range 17.0−1.0, indicating the presence of an exchange interaction between the Co(II) ions.

An important piece of information pertaining to the nature of the exchange interaction emerges from the g values of the single Co(II) ion: if $g_z > g_x, g_y$, the ion is closer to the Ising limit. If $g_x, g_y > g_z$, the system is closer to the XY limit. The conditions for observing $g_z > g_x, g_y$ were given earlier by Abragam and Bleaney, using a crystal field approach.[67] It was, then, found that in the Ising limit $g_z = 8-9$ and $g_x = g_y = 0$, while for the XY limit $g_{xy} = 4$ and $g_z = 2$. The values observed here for complex **1** are beyond every limit, thus indicating that an interaction between the two Co(II) octahedral centers does arise.

It is interesting to note that, in solution, the dimer seems to dissociate into monomers, in view of the fact that the derived signal exhibits an isotropic g value equal to 4.21 followed by a broad peak at $g = 2.2$. This picture is consistent

(65) Casan-Pastor, N.; Serra, J. B.; Coronado, E.; Pourroy, G.; Baker, L. C. W. *J. Am. Chem. Soc.* **1992**, *114*, 10380–10383.
(66) Garcia, C. J. G.; Coronado, E.; Almenar, J. B. *Inorg. Chem.* **1992**, *31*, 1667–1673.
(67) Abragam, A.; Bleaney, B. *Electron Paramagnetic Resonance of Transition Ions*; Clarendon Press: Oxford, U.K., 1970.

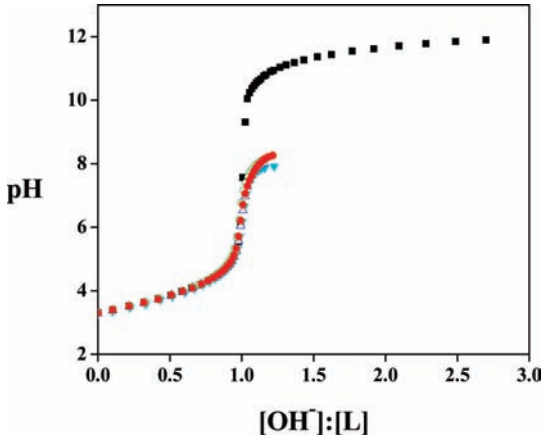

Figure 8. Potentiometric titration curves of free quinic acid (■) and Zn(II)−quinic acid with different molar ratios: (▼) c_{Zn} = 0.004067 mol dm^{-3}, c_{ligand}=0.00403 mol dm^{-3}; (△) c_{Zn}=0.002033 mol dm^{-3}, c_{ligand} = 0.00403 mol dm^{-3}; (○) c_{Zn} = 0.001383 mol dm^{-3}, c_{ligand} = 0.00403 mol dm^{-3}; (●) c_{Zn} = 0.001017 mol dm^{-3}, c_{ligand} = 0.00403 mol dm^{-3}.

with previous observations on the EPR behavior of the binary Co(II)−(D-(−)-quinic acid) system.[35]

Speciation Studies. Potentiometric titrations of the free ligand D-(−)-quinic acid as well as Zn(II) with D-(−)-quinic acid in various molar ratios were carried out. Some of the derived titration curves, both experimental and calculated, are shown in Figure 8. The titration curves were evaluated with different potential speciation models. Nevertheless, the best fit arising among the experimental and calculated titration curves for the binary Zn(II)−quinic acid system was obtained by considering the species $[Zn]^{2+}$; $[ZnL_2]^0$, where LH = $C_7H_{12}O_6$ and L = $C_7H_{11}O_6^-$; $[ZnL_2H_{-1}]^-$; and finally $[ZnH_{-1}]^+$.

Other complexes including oligonuclear species, such as 2:1 or 3:1 Zn(II)/quinate complexes or variably protonated and deprotonated species, were rejected by the computer program (PSEQUAD) during the computational process. The species emerging from the speciation distribution of the binary system are in line with the species synthesized and isolated in the solid state. It is worth stating that the same speciation model was established in similar binary systems, including Co(II)−quinate[35] and Ni(II)−quinate.[54] The stability constants of the complexes formed are listed in Table 4. The uncertainties (3SD values) for the stability constants are given in parentheses. The pH range of the optimal formation of complexes is also reported. For the titratable quinate carboxylate group, the pK_a value of 3.34 was obtained and was found to be very close to the values reported by Clifford (3.40)[68] and Luethy-Krause et al. (3.36).[69] For shikimic acid (3*R*,4*S*,5*R*)-3,4,5-trihydroxy-1-cyclohexanecarboxylic acid), the pK_a value is 4.15. The presence of an alcoholic moiety in a position α to the carboxylate group of quinic acid increases its acid strength.

The titrimetric data were evaluated on the premise that complex formation between Zn(II) and quinate proceeds through binding of the quinate carboxylate moiety and the alcoholic group. The titration curves in the absence and presence of Zn(II) suggest formation of the complexes

(68) Clifford, M. *Tea Coffee Trade J*. **1987**, *159*, 35–39.
(69) Luethy-Krause, B.; Pfenninger, I.; Landolt, W. *Trees Struct. Funct*. **1990**, *4*, 198–204.

Table 4. Proton (log *K*) and Zn(II)−Quinic Acid Complex Formation Constants (log *β*) at *I* = 0.15 M (NaCl) and 25 °C[a]

	quinic acid (QA)	Zn(II)−QA	pH range for each species
log K(HL)	3.34(1)		
log *β* (ZnL_2)		4.23(3)	entire domain
log *β* (ZnL_2H_{-1})		−3.08(8)	>6.5
p*K* ($[ZnL_2H_{-1}]/[ZnL_2]$)		7.31	
fitting[b]		4.861×10^{-2}	
no. of pts.		129	

[a] Charges from the various species are omitted for clarity. [b] Goodness of fit between the experimental and the calculated titration curves expressed in milliliters of titrant.

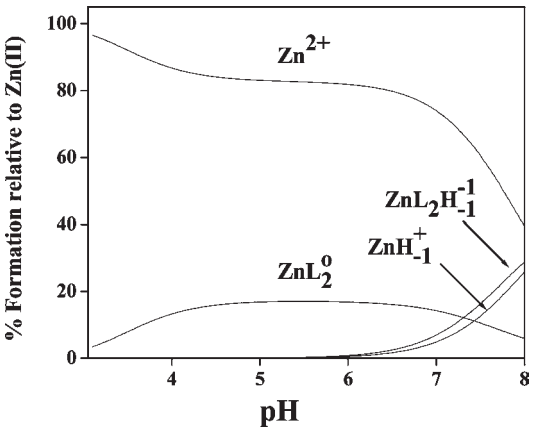

Figure 9. Speciation curves for complexes forming in the Zn(II)−quinic acid system; c_{Zn} = 1.38 mmol dm^{-3}, c_{ligand} = 4.03 mmol dm^{-3}. Charges are omitted for clarity.

$[Zn]^{2+}$ and $[ZnL_2]^0$, in the acidic region up to pH 7−7.5, and of $[ZnL_2H_{-1}]^-$ at pH values beyond 6.5 (Figure 9). The studies also suggest that this ligand reacts expediently with Zn(II) ions, forming soluble metal chelate complexes. Similar complex species were observed in the speciation model of the Zn(II)/orotic acid system.[20] The Zn(II) ion is not sufficiently strong to deprotonate the alcoholic oxygens of the quinate ligand. Therefore, in congruence with the solid state structure (Figure 3), which shows only the carboxylate group being deprotonated, the mononuclear complex $[ZnL_2]^0$ contains the singly deprotonated ligand bound to the metal ion. This species forms in the entire pH range investigated, with a maximum of 20% at a pH of 4.5−6.5, and it coexists with the hexa-aquo Zn(II) species $[Zn(H_2O)_6]^{2+}$ over the entire pH domain (Figure 9). The species distribution in Zn(II) complexes formed by fibrinopeptide A shows the presence of more than 95% free Zn^{2+} up to a pH of 7 even with a molar ratio L/Zn = 5:1.[70] The presence of the hexa-aquo $[Zn(H_2O)_6]^{2+}$ species over the entire pH range investigated or over a wide pH range was also observed in some aqueous systems of Zn(II) with N-acetyl-His-Pro-His-His-NH_2 at a pH of 4−7,[71] 2-hydroxynicotinic acid at a pH of 2−7,[21] (2-amino-2-phenyl-1-hydroxy)ethyl phosphonic acid at a pH of 2−9,[72] L-aspartyl-L-alanyl-L-histidine-*N*-methyl amide and glycylglycyl-L-histidine-*N*-methyl

(70) Galey, J.-F.; Kozlowski, H.; Pettit, L. D. *J. Inorg. Biochem*. **1991**, *44*, 149–153.
(71) Jakab, N. I.; Jancso, A.; Gajda, T.; Gyurcsik, B.; Rockenbauer, A. *J. Inorg. Biochem*. **2008**, *102*, 1438–1448.
(72) Gumienna-Kontecka, E.; Gałezzowska, J.; Drazg, M.; Latajka, R.; Kafarski, P.; Kozłowski, H. *Inorg. Chim. Acta* **2004**, *357*, 1632–1636.

amide at a pH of 5−8.5,[73] the cyclic dipeptides c-HisCys at a pH of 2−7,[74] and N(α)-acetylcysteine at a pH of 2−8.[75]

The overall stability constant of the mononuclear complex $[ZnL_2]^0$ ($\log\beta = 4.23$) is closer to that of similar complexes of Zn(II) with α-hydroxycarboxylic acids, such as 2-hydroxyacetic acid (glycolic acid; $\log\beta = 2.70$),[76] 2-hydroxypropanoic acid (lactic acid; $\log\beta = 3.04$),[77] 2-hydroxybutanoic acid ($\log\beta = 3.02$),[78] 2-hydroxy-2-methylpropanoic acid (2-hydroxyisobutyric acid; $\log\beta = 2.97$),[79] and 2-hydroxy-2-phenylacetic acid (mandelic acid; $\log\beta = 2.58$).[80] Also, the overall stability constant of $[ZnL_2]^0$ is in line with the corresponding constant of the analogous quinate complexes of Co(II) ($\log\beta = 4.34$)[35] and Ni(II) ($\log\beta = 4.95$).[54]

At pH values beyond 6.5 in the binary Zn(II)−quinic acid system, both (a) the mononuclear species $[ZnL_2H_{-1}]^-$ and (b) the mononuclear species $[Zn(OH)]^+$ are present, as in the case of the aqueous quinate system with Co(II)[35] and Ni(II).[54] In the $[ZnL_2H_{-1}]^-$ species, however, one of the two quinate ligands bound to the Zn(II) is probably deprotonated at the alcoholic group adjacent to the carboxylate group or one of the two coordinated water molecules in $[ZnL_2]^0$. The overall stability constant of the $[ZnL_2H_{-1}]^-$ ($\log\beta = -3.08$) species is similar to the overall stability constant of the same species in the aqueous binary Co(II)−quinic acid[35] and Ni(II)−quinic acid[54] systems. The Zn(II) ion exhibits a relatively strong tendency to form hydroxo complexes and even precipitates, creating problems in the interpretation of Zn(II) complex chemistry.[81] Over the pH range 7.9−8.25, depending on the molar ratio of Zn(II)/quinic acid in the binary system of Zn(II) with quinic acid, a precipitate appears and the pH rise ceases, most likely because OH^- ions are consumed toward the formation of $Zn(OH)_2$. The incipient precipitation at pHs beyond 8.25 makes the observation of the next step doubtful, even in the presence of a higher ligand-to-metal molar ratio.

A similar speciation model arose for the 1:1 ZnL case (see the Supporting Information). The adopted speciation model considered the species $[Zn]^{2+}$, $[ZnL]^+$ (LH = $C_7H_{12}O_6$; L = $C_7H_{11}O_6^-$), $[ZnLH_{-1}]^0$, and $[ZnH_{-1}]^+$. The fit is reasonably good in the overall pH and concentration range used, demonstrating that the adopted speciation model is satisfactorily defined ($f = 0.05829$). To this end, the two speciation models are reasonably good, and they suggest that additional information may be needed to select the one more representative of the solution picture. ESI-MS spectroscopy was crucial in that respect, pointing out the species present in aqueous solutions of Zn(II) and quinic acid. Solution mixtures of Zn(II) (solution A) and quinic acid (solution B) in molar stoichiometries of 1:1 and 1:2 showed that the species present is the 1:2 ($m/z = 447.075$, $z = 1$), very likely reflecting the ZnL_2 species proposed by the aqueous speciation model presented above (see the Discussion). In the analogous case of the Co(II)−quinic acid binary system, ESI-MS spectroscopy was critical in establishing the presence of the 1:2 CoL_2 species, which was subsequently synthesized, isolated, and characterized.[35] Analogous synthetic attempts are currently in progress in the case of the corresponding zinc species.

Discussion

Chemical Reactivity and Interconversions in Co(II)−Quinate Structural Chemistry. The variable reactivity of Co(II) toward D-(−)-quinic acid exemplifies once again the chemical affinity of D-(−)-quinic acid for divalent metal ions such as Co(II). Undoubtedly, the pH of the reaction solution (absence of base) as well as the reaction temperature in the investigated binary system was crucial in promoting the presented reactions and finally the isolation of discrete crystalline products in a suitable form for further characterization. The analytical, spectroscopic, and structural characterization of the isolated inorganic−organic hybrid $[Co_2(C_7H_{11}O_6)_4]_n \cdot nH_2O$ (**1**) reflected (a) the physical and chemical properties of **1** dictated by pH and the employed hydrothermal conditions and (b) the basis of potential transformations and linkage of **1** with various mononuclear binary partner Co(II)−quinate species.

Therefore, compound **1** provides a well-defined example of a binary M(II)−quinate material (a) accessible through the hydrothermal synthesis between a divalent metal ion and an α-hydroxycarboxylate ligand, (b) gaining stability upon chelation of the α-hydroxycarboxylate moiety of a quinate ligand binding Co(II) and the formation of five-membered cyclic rings, (c) characterized by the presence of α-hydroxycarboxylate bound to Co(II), with the alcoholic group adjacent to the carboxylic acid moiety retaining its proton—protonation of the α-hydroxy group of the quinate ligand has also been observed in the case of the previously isolated and characterized mononuclear Co(II)−quinate species as well as in the case of other divalent or trivalent metal−quinate complexes, including Mn(II),[53] Ni(II),[54] and Fe(III)[82]—and (d) possessing one of the quinate triol functionalities participating in metal binding, thereby promoting the formation of polymeric and/or polynuclear species. In this regard, **1** is the first of the Co(II)−quinate family of species, where one of the protonated triol moieties plays a key role in the formation of polymeric species, similar to isostructural $[Mn_2(C_7H_{11}O_6)_4]_n \cdot nH_2O$.[53] In the latter case, however, no analogous aqueous transformation chemistry had been shown to link the dinuclear repeating unit with mononuclear partners of variable composition.

Magnetic susceptibility studies of **1** revealed the presence of distinct high-spin Co(II) ions in an octahedral crystal field, and the EPR spectrum provided information about the (a) solid state signature of **1**, (b) comparison of the spin signature with that of the Mn(II) counterpart, and (c) integrity of **1** in solution. The studies suggest that **1** dissociates upon dissolution in an aqueous medium and does not retain its structure in solution. The frozen

(73) Lakusta, H.; Sarkar, B. *J. Inorg. Biochem.* **1979**, *11*, 303–315.
(74) Gockel, P.; Vogler, R.; Gelinsky, M.; Meissner, A.; Albrich, H.; Vahrenkamp, H. *Inorg. Chim. Acta* **2001**, *323*, 16–22.
(75) Gockel, P.; Vahrenkamp, H. *Helv. Chim. Acta* **1993**, *76*, 511–520.
(76) Pushparaja, B.; Sudersanan, M. *Indian J. Chem.* **1980**, *19A*, 149.
(77) Lepri, L.; Desideri, P. G. *J. Chromatogr.* **1973**, *84*, 155–164.
(78) Filipovic, I.; Piljac, I.; Bach-Dragutinovic, B.; Kruhak, I.; Grabaric, B. *Croat. Chem. Acta* **1973**, *45*, 447–452.
(79) Lengyel, T. *Acta Chim. Acad. Sci. Hung.* **1969**, *60*, 373.
(80) Matusinovic, T.; Filipovic, I. *Croat. Chem. Acta* **1985**, *58*, 227.
(81) Martin, R. B. *Prod. Natl. Acad. Sci. U.S.A.* **1974**, *71*, 4346–4347.
(82) Menelaou, M.; Mateescu, C.; Zhao, H.; Rodriguez-Escudero, I.; Lalioti, N.; Sanakis, Y.; Simopoulos, A.; Salifoglou, A. *Inorg. Chem.* **2009**, *48*, 1844–1856.

solution EPR spectrum of **1** was shown to be identical to that of $[Co(C_7H_{11}O_6)_2(H_2O)_2]$,[35] thereby attesting to the identity of species in water as $[CoL_2]$. In a similar fashion, the frozen solution EPR spectrum of the anionic species $[CoL_3]^-$ isolated in the solid state was shown to be the same as that of $[CoL_2]^0$.[35] Further proof of that observation had been previously provided by ESI-MS spectroscopy in aqueous solutions of (a) the dissolved $[CoL_2]^0$ species and (b) Co(II) and quinic acid reacting at various molecular stoichiometries. Hence, the suggestion that the mononuclear $[CoL_2]^0$ species is the dominant species in aqueous solutions of the Co(II)−quinate family, as previously reported, is herewith being enhanced.

On the basis of the above revelations, rational synthetic transformations were examined, emphasizing the possible chemical link between various species arising from the binary Co(II)−quinate system. For that reason, two different chemical pathways were followed. As shown in Scheme 1, the dominant species clearly proved to be the mononuclear species $[CoL_2]^0$. Therefore, under various synthetic procedures (a) the anionic complex $[CoL_3]^-$ and (b) the dinuclear species $[Co_2L_4]^0$ were isolated. Furthermore, another successful transformation was accomplished; the starting compound was the inorganic−organic hybrid $[Co_2L_4]^0$ and, as is depicted in Scheme 1, the aqueous transformation led to the $[CoL_2]^0$ species, indicating the close relationship between the two Co(II)−quinate species. The demonstrated transformation work emphasizes the importance of solid-state-solution structure correlation, targeting specific binary interactions with physiological D-(−)-quinic acid and metal ions like Co(II) and Zn(II). The employment of such simple binary M(II)−quinate mononuclear species as precursors in the assembly of higher nuclearity materials is a task currently under investigation.

The Structural Speciation of the Binary M(II)−Quinic Acid System. The physicochemical properties of the binary Zn(II)−D-(−)-quinic acid system were studied thoroughly in the solid state and in solution. To this end, the aqueous speciation studies in the binary Zn(II)−quinate system (a) contribute to the understanding of the nature of various species forming as a function of pH and reagent molar stoichiometry and (b) provide a direct correlation of the physicochemical profile of the proposed species with the structure and properties of the species synthesized and isolated, $[Zn_3(C_7H_{11}O_6)_6]_n \cdot nH_2O$ (**2**). The considered potential speciation models suggest the presence of either 1:1 ZnL or 1:2 ZnL_2 species in solution (among others). Combined solution speciation studies and ESI-MS spectroscopy suggest that the likely speciation model is the one containing the 1:2 ZnL_2 species. To this end, confirmation supporting the aqueous speciation data and the identity of the proposed species comes from ESI-MS spectroscopy (m/z = 447.075, z = 1, $[ZnL_2 + H]^+$). Therefore, the likely binary species prevailing in the aqueous speciation of the investigated binary system appears to be the one bearing a 1:2 Zn/L stoichiometry. In line with this stoichiometry, mononuclear ($[ZnL_2]^0$, $[ZnL_2H_{-1}]^-$) species emerge as competent participants in the pH distribution. The proposed speciation distribution for Zn(II) is in line with the corresponding speciation distributions previously observed in the case of Co(II)[35] and Ni(II).[53] Of the two species, the $[ZnL_2]^0$ complex reflects quite well the molecular stoichiometry of the species synthesized and isolated in the solid state (**2**). It could be envisioned that **2** may arise through substitution of the water molecules bound to Zn(II) in $[ZnL_2]^0$ by adjacently located similar units, utilizing the anchoring ability of the second oxygen terminal of the carboxylate group bound to Zn(II). Such a tentative reactivity scheme may be the result of the reaction conditions during hydrothermal synthesis at elevated temperatures (160 °C). Support for such a case would be the synthesis and isolation of species such as $[ZnL_2]^0$. Efforts are currently under way to synthesize and isolate species reflected in $[ZnL_2]^0$ and $[ZnL_2H_{-1}]^-$.

In the analogous case of $[Co_2(C_7H_{11}O_6)_4]_n \cdot nH_2O$ (**1**), the Co/L 1:2 stoichiometry reflected in the solid state species projects analogous reactivity between Co(II) and quinic acid under the prevailing reaction conditions during hydrothermal synthesis. Here too, the solid state species **1** gives rise to CoL_2 in solution, with the presence of such a species being attested to by (a) ESI-MS and EPR in solution speciation studies and in solutions resulting upon dissolution of **1** and (b) synthetic procedures leading to the isolation of the actual complex CoL_2 in the solid state followed by X-ray crystallographic characterization.

2D Lattice Architecture vs M(II)−Quinate Materials. In both **1** and **2**, hydrothermal synthesis provides a strategy to achieve solid state metal−organic lattices of (a) specific dimensionality, (b) composition and architecture, and (c) physicochemical properties that either differentiate the isolated species from already known species within the same binary system[35] or project unique materials that otherwise might not have been possible to synthesize. To this end, hydrothermal techniques have proven to be very successful in the synthesis of coordination polymers. The reactivity chemistry in each of the investigated binary systems coupled with the inherent structural properties of quinate lead to specific lattice architectures (in **1** and **2**), reflecting the reactivity of the specific metal ion and the ligand bound to it in a distinct coordination mode. In their respective solid-state lattice, the two-dimensional arrangement of Co(II) (**1**) and Zn(II) (**2**) complex units reveals that the employed reaction conditions very likely direct the specific and unique assembly of the corresponding complexes, taking into consideration the structure and coordination mode of the ligand, the pH, the charge distribution on the arising quinate moiety, and the potential emergence of variable strength H-bond and hydrophobic−hydrophilic forces, among other factors. Given the multicomponent nature of quinate and thus the diverse modes it can adopt when reacting with metal ions, it appears that a variety of factors (such as those emerging in hydrothermal synthesis) can influence the mechanistic pathway leading to the assembly of 2D metal−organic lattices such as those in **1** and **2**. It would not be surprising if carefully selected reaction conditions within the binary Co(II)/Zn(II)−quinate system influence specific pathways leading to new and elusive polymeric or discrete nonpolymeric metal−organic materials of unique lattice composition, nuclearity, dimensionality (1D−3D), and properties (magnetostructural, spectrochemical, etc.). An investigation of approaches attempting to deconvolute such interwoven relationships (between metal−ligand interacting factors and synthetic reaction conditions) influencing lattice assembly processes in binary M(II)−hydroxycarboxylate systems is under way in the lab.

Conclusions. The pH-specific synthetic chemistry presented herein exemplifies the diversity of reactivity conditions under which D-(−)-quinic acid can interact with metal ions such as Co(II) and Zn(II) to yield well-defined materials. Compounds **1** and **2** have distinct chemical and structural properties in the solid state and in solution, thereby allowing for ensuing ternary interactions with third partners under specific reaction conditions. To this end, the hydrothermal conditions used for the synthesis and isolation of the M(II)−(O)-containing materials **1** and **2** may pave the way to new oligo- or multinuclear materials, starting from simple reagents (synthons) not unlike those in **1** and **2**. Such species (a) are proposed through the aqueous speciation in the binary Co(II)/Zn(II)−quinate system, and (b) can serve as precursors to new variable nuclearity compounds that could be isolated from the binary [Co(II),Zn(II)]−quinate systems, under hydrothermal or solvothermal conditions, with distinct chemical properties and lattice architecture. In this regard, further in-depth work seeking to discover well-defined links between variably structured α-hydroxycarboxylate ligands and divalent Co(II) and Zn(II) are warranted and are currently under investigation in our lab.

Acknowledgment. This work was supported by a "Pythagoras" grant from the National Ministry of Education and Religious Affairs and by a "PENED" grant from the General Secretariat of Research and Technology, Greece.

Supporting Information Available: X-ray crystallographic data in CIF format for $[Co_2(C_7H_{11}O_6)_4]_n \cdot nH_2O$ (**1**) and $[Zn_3(C_7H_{11}O_6)_6]_n \cdot nH_2O$ (**2**). UV−visible spectrum of **1** in water. Speciation curves for complexes forming in the binary Zn(II)−quinic acid system. Full scan MSs of a mixture of solutions. Proton (log *K*) and Zn(II)−quinic acid complex formation constants. Bond lengths [Å] and angles [deg] of **1** and **2**. Hydrogen bonds in **1** and **2**. The material is available free of charge via Internet at http://pubs.acs.org.